Supporting Information (SI)

Facile low-temperature synthesis of hematite quantum dots anchored on three-dimensional ultra-porous graphene-like framework as advanced anode materials for asymmetric supercapacitors

Yunyong Li[a], Haiyan Zhang[a,] *, Shanxing Wang[a], Yingxin Lin[a], Yiming Chen[a], Zhicong Shi[a], Na Li[a], Wenguang Wang[a], and Zaiping Guo[a, b,] *

[a]*Guangdong Provincial Key Laboratory of Functional Soft Condensed Matter, School of Materials and Energy, Guangdong University of Technology, No. 100 Waihuan Xi Road, Guangzhou Higher Education Mega Center, Guangzhou 510006, China*

[b]*Institute for Superconducting and Electronic Materials, School of Mechanical, Materials and Mechatronics Engineering, University of Wollongong, North Wollongong, New South Wales 2500, Australia*

[a,] *Corresponding author. Tel.: +86 20 39322570, Fax: +86 20 39322570, *E-mail address:* yyli@gdut.edu.cn *(Y. Y. Li)*, *hyzhang@gdut.edu.cn (H. Y. Zhang).*

[a, b,] *Corresponding author. Tel.: +61 2 4221 5225, Fax: +61 2 4221 5731, *E-mail address: zguo@uow.edu.au (Z. P. Guo).*

Experimental section

Synthesis of the 3D GF

The 3D GF was synthesized by an improved procedure according to our previous work[S1]. In brief, pre-treated macroporous acrylic type cation-exchange resin was firstly impregnated with 0.10 mol L^{-1} nickel acetate solution (100 mL). The nickel ion-exchange resin was washed and dried. Then, the nickel ion-exchange resin (10 g) was added under stirring into 400 mL KOH/ethanol solution containing 45 g KOH and dried to form a nickel ion-exchange resin/KOH mixture. Finally, the mixture was heated at 850 ^{o}C for 2 h in N_2 atmosphere with a heating rate of 2 ^{o}C min^{-1}. After cooling down to room temperature, the resulting sample was treated in 3 mol L^{-1} HCl solution to remove the nickel nanoparticles and other impurities. The sample was finally washed and dried. The 3D GF powders were vacuum dried at 120 ^{o}C for 5 h.

Calculation methods of supercapacitors in three-electrode and two-electrode systems

Three-electrode system. The gravimetric capacitance C_g (F g^{-1}) of the active material could be calculated from the corresponding cyclic voltammetry curve by the following equation[S2, S3]:

$$C_g = \frac{\int I(V)\,\mathrm{d}V}{2vm\Delta V} \qquad \text{(S1)}$$

where $I(V)$ (A) is the response current, V (V) is the potential *vs.* Hg/HgO reference electrode, v (V s^{-1}) is the scan rate, m (g) is the mass of the active material (including the mass of 3D GF) on the working electrode, and ΔV (V) is the range of working

potential.

For the non-linear galvanostatic charging and discharging (GCD) plots: C_g (F g^{-1}) could be calculated using the following equation[S4, S5]:

$$C_g = \frac{2I_m \int V dt}{V^2 \Big|_{V_i}^{V_f}} \qquad \text{(S2)}$$

where $I_m = I/m$ (A g^{-1}) is the current density, I (A) is the current, and m (g) is the mass of the active material (including the weight of 3D GF) on the working electrode, $\int Vdt$ is the integral current area, where V (V, taking absolute value, here is 0.6 V) is the potential, with initial and final values of V_i and V_f, respectively.

For the linear GCD plots: C_g (F g^{-1}) could be calculated using the following equation:

$$C_g = \frac{I\Delta t}{m\Delta V} \qquad \text{(S3)}$$

where I (A) is the current, Δt (s) is the charging time, m (g) is the mass of the active material on the working electrode, and ΔV (V) is the range of working potential.

Two-electrode system. The specific capacitance C_{ASC} (F g^{-1}) of the ASC device could be calculated from the corresponding galvanostatic discharging curve according to the following equation:

$$C_{ASC} = \frac{I\Delta t}{M\Delta V} \qquad \text{(S4)}$$

where I (A) is the discharging current, Δt (s) is the discharging time, ΔV (V) is the potential window during discharging, M (g) is the total mass of active materials in the ASC device. The equivalent series resistance (R_{ESR}) (Ω) of the device could be calculated by:

$$R_{\mathrm{ESR}} = \Delta V_{\mathrm{drop}}/(2I) \qquad \text{(S5)}$$

where ΔV_{drop} (V) is the abrupt voltage drop at the beginning of the discharging curve,

I (A) is the corresponding current. The energy density E (Wh kg^{-1}) and average power density P (W kg^{-1}) could be calculated as:

$$E = \frac{0.5 C_{ASC} V^2}{3.6} \qquad \text{(S6)}$$

$$P = E/t \qquad \text{(S7)}$$

where V (V) is the potential of the ASC and t (s) is the corresponding discharging time.

The maximum power density (P_{max}) calculated from R_{ESR} and normalized by the mass of the cell (two electrodes) is given by $P_{max} = V^2/(4mR_{ESR})$.

Additional results:

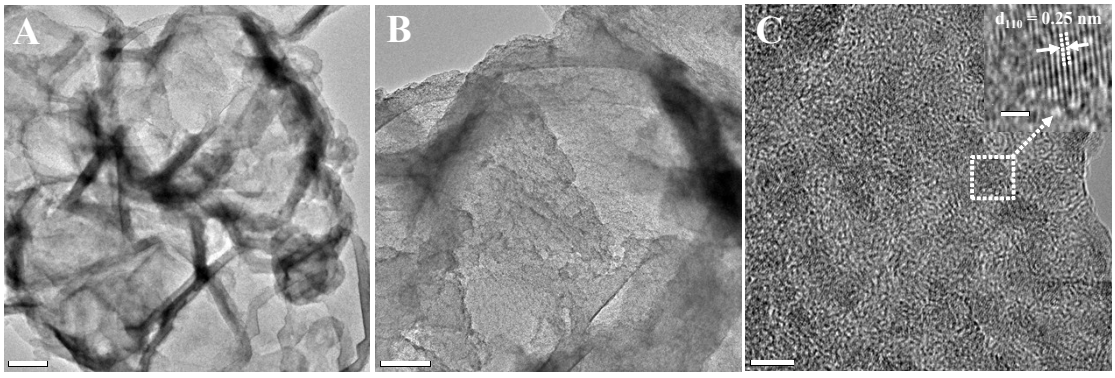

Fig. S1 (A, B) TEM images and (C) high-resolution TEM image of Fe_2O_3-QDs-3D GF hybrid composite. Inset in (C) is an enlarged view corresponding to the area outlined by the white square.

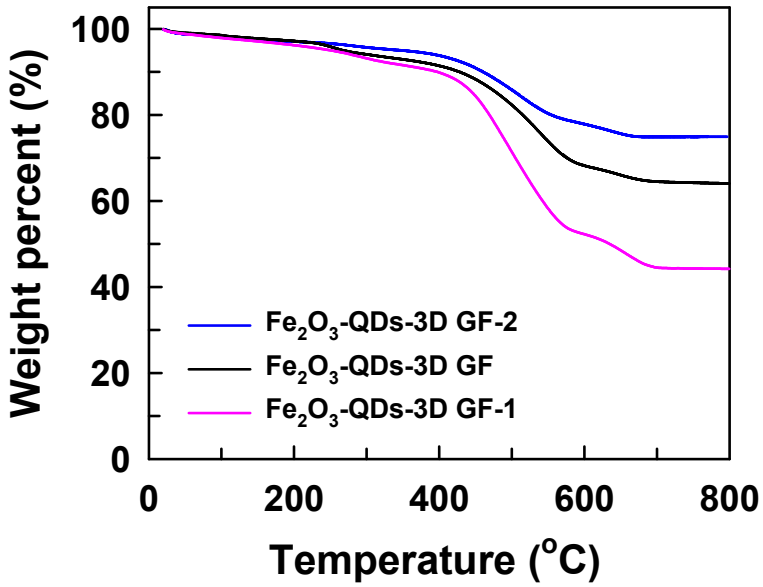

Fig. S2 Thermogravimetric analysis (TGA) of three Fe_2O_3-QDs-3D GF composites with different contents of Fe_2O_3-QDs. The TGA was conducted under air at a heating rate of 10 °C min^{-1} from room temperature to 800 °C. The contents of Fe_2O_3 in the three Fe_2O_3-QDs-3D GF composites were calculated by TGA, which are ~74.9 wt%, ~64.1 wt%, and ~44.2 wt%, respectively.

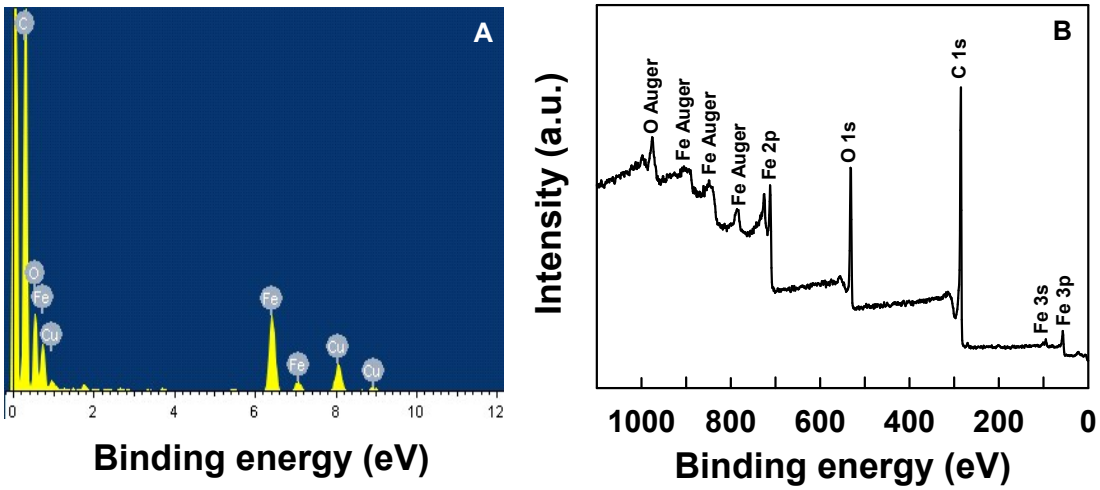

Fig. S3 EDS spectrum (A) and XPS survey spectrum (B) of Fe_2O_3-QDs-3D GF composite.

The TEM-based EDS spectrum and the XPS survey spectrum in Fig. S3 further

demonstrate that only C, O, and Fe exist in the composite, while the Cu is derived from the copper grid. The results further confirm the successful deposition of Fe_2O_3-QDs on the 3D GF.

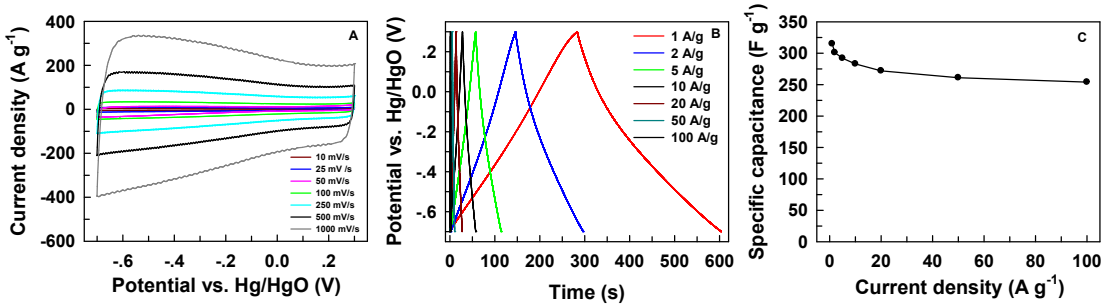

Fig. S4 Electrochemical performance of 3D HPG in three-electrode system in 2 mol L^{-1} KOH aqueous solution. (A) CV curves at various scan rates, (B) galvanostatic charge/discharge curves at different current densities, and (C) specific capacitance as a function of current density.

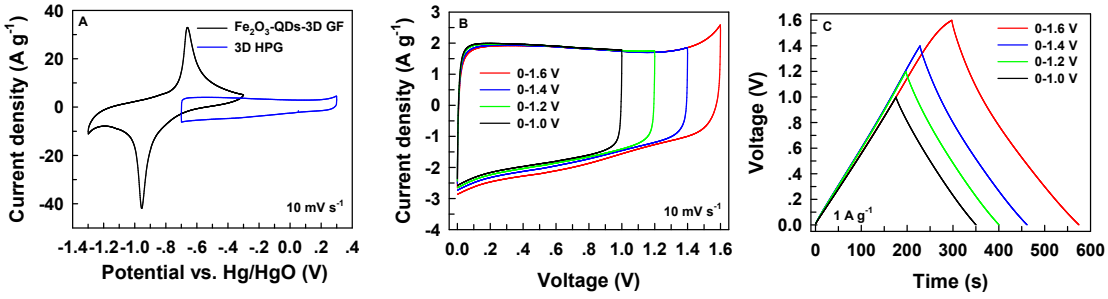

Fig. S5 (A) CV curves of 3D HPG and Fe_2O_3-QDs-3D GF electrodes in the three-electrode system in 2.0 mol L^{-1} KOH aqueous solution at 10 mV s^{-1}. (B) CV curves and (C) galvanostatic charge/discharge curves of Fe_2O_3-QDs-3D GF//3D HPG ASC at 1.0 A g^{-1}.

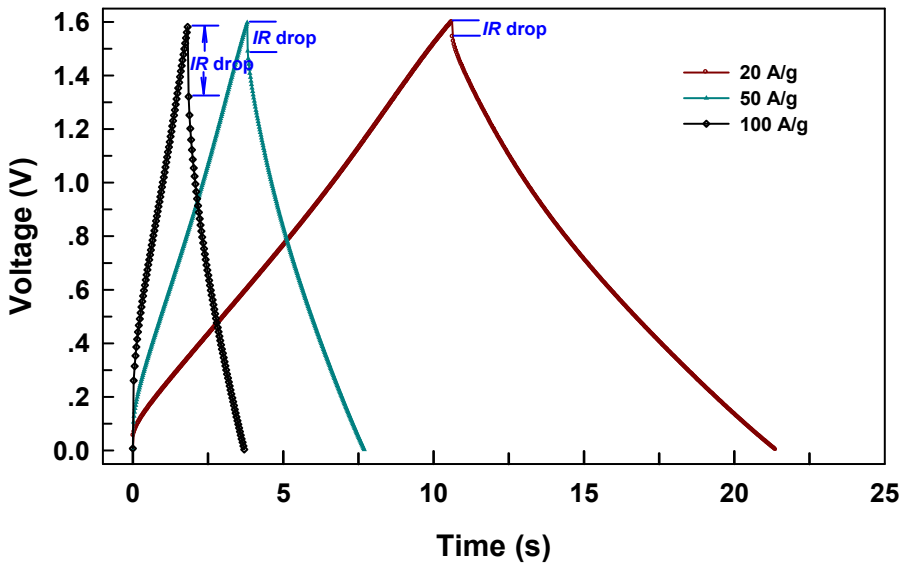

109

110 **Fig. S6** Galvanostatic charge/discharge curves and *IR* drops of Fe_2O_3-QDs-3D

111 GF//3D HPG ASCs at various high current densities.

112

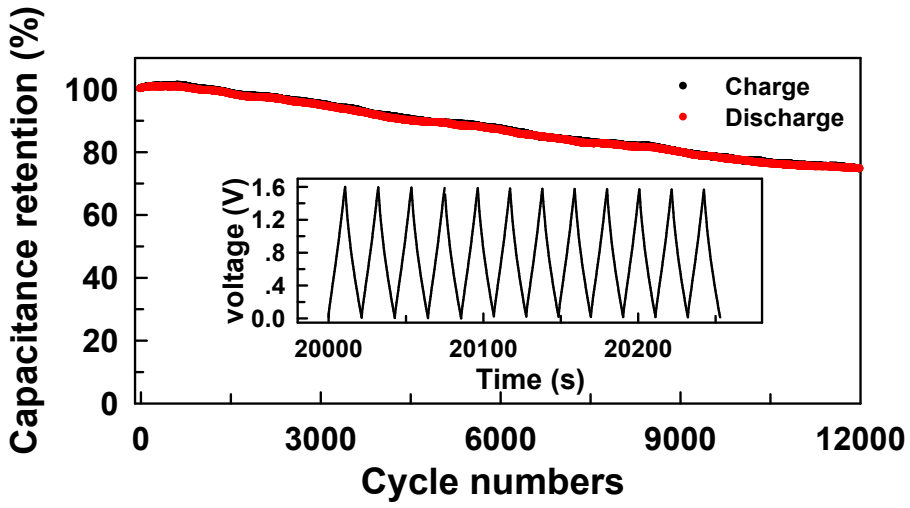

113

114 **Fig. S7** Cycling stability test at current density of 20 A g^{-1} for Fe_2O_3-QDs-3D GF//3D

115 HPG ASC after the test for 10000 cycles at 2.0 A g^{-1}. Inset shows the stability of the

116 voltage as a function of time.

117

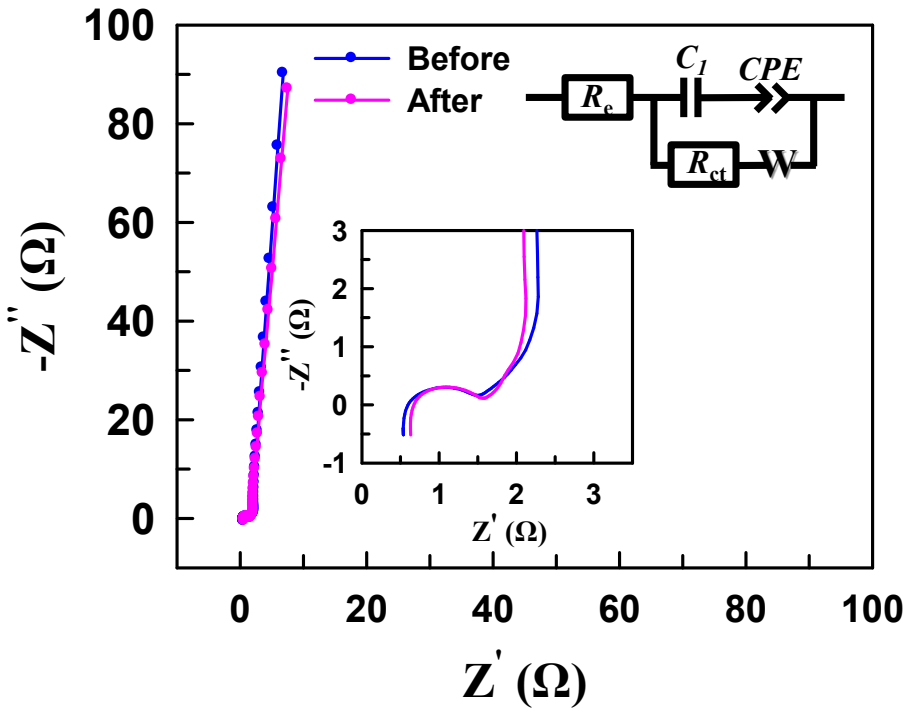

Fig. S8 Nyquist plots and their expanded high-frequency region (lower inset) of an Fe_2O_3-QDs-3D GF//3D HPG ASC before and after cycling stability testing for 12000 cycles at 20 A g^{-1} (measured in the frequency range of 100 kHz - 0.01 Hz at open circuit potential with an ac perturbation of 5 mV). The upper inset in Fig. S8 is the equivalent circuit. R_e stands for the combined ionic resistance of the electrolyte, intrinsic resistance of the substrate, and contact resistance at the active material/current collector interface, while R_{ct} is charge-transfer resistance caused by the Faradaic reactions and the double-layer capacitance on the grain surface. C_1 is the double layer capacitance, W is the Warburg impedance, and CPE represents the constant phase element.

Table S1 Physical characteristics of 3D GF, three Fe_2O_3-QDs-3D GF composites, and pure Fe_2O_3.

Samples	BET total surface area ($m^2\ g^{-1}$)	Total pore volume ($cm^3\ g^{-1}$)	Conductivity ($\times 10^3\ S\ m^{-1}$)
3D GF	2250	1.38	1.40
Fe_2O_3-QDs-3D GF-1	1159	0.86	1.31
Fe_2O_3-QDs-3D GF	734	0.58	1.25
Fe_2O_3-QDs-3D GF-2	507	0.42	0.95
Pure Fe_2O_3	18	0.06	---

Table S2 Comparison of the electrochemical performances of different Fe_2O_3/graphene-based electrodes.

Electrode material	*SSA* ($m^2\ g^{-1}$)[a]	Electrolyte	[c]Calculation methods for [b]C_g	C_g ($F\ g^{-1}$)	Rate capability ($F\ g^{-1}$)	Year and Ref.
Graphene/Fe_2O_3/polyaniline		1 M KOH	$C_g = \frac{I\Delta t}{m\Delta V}$	638 at 1.0 mV s^{-1}		2012[S6]
Graphene/Fe_2O_3 nanorods	87.9	6 M KOH	$C_g = \frac{I\Delta t}{m\Delta V}$	320 at 10 mA cm^{-2}	152 at 100 mA cm^{-2}	2013[S7]
Fe_2O_3/graphene	357.6	1 M Na_2SO_4	$C_g = \frac{I\Delta t}{m\Delta V}$	226 at 1.0 A g^{-1}	90.8 at 5 A g^{-1}	2013[S8]
Fe_2O_3/N-rGO hydrogel	171.5	1 M KOH	$C_g = \frac{I\Delta t}{m\Delta V}$	618 at 0.5 A g^{-1}	350 at 10 A g^{-1}	2014[S9]
α-Fe_2O_3 mesocrystals/graphene	89.1	1 M Na_2SO_4	$C_g = \frac{I\Delta t}{m\Delta V}$	306.9 at 3.0 A g^{-1}	98.2 at 10 A g^{-1}	2014[S10]
Graphene/Fe_2O_3	173	1 M KOH	$C_g = \frac{I\Delta t}{m\Delta V}$	908 at 2.0 A g^{-1}	~700 at 30 A g^{-1}	2014[S11]
N-rGO/Fe_2O_3	56.2	1 M KOH	$C_g = \frac{I\Delta t}{m\Delta V}$	268.4 at 2.0 A g^{-1}	137.0 at 5 A g^{-1}	2015[S12]
Porous Fe_2O_3/graphene	95.9	1 M Na_2SO_4	$C_g = \frac{I\Delta t}{m\Delta V}$	343.7 at 1.0 A g^{-1}	182.1 at 10 A g^{-1}	2015[S13]
G-Fe_2O_3	127.8	3 M KOH	$C_g = \frac{I\Delta t}{m\Delta V}$	1095 at 3.0 A g^{-1}	506.6 at 30 A g^{-1}	2015 [S3]
Fe_2O_3/FGS	208	1 M Na_2SO_4	$C_g = \frac{I\Delta t}{m\Delta V}$	347 at 10 mV s^{-1}	140 at 1600 mV s^{-1}	2015[S14]

GF-CNT@400Fe_2O_3		2 M KOH	$C_g = \frac{I\Delta t}{m\Delta V}$	580.6 at 5 A g^{-1}	370.2 at 40 A g^{-1}	2015[S15]
rGO/PEDOT:PSS/α-Fe_2O_3	269	1 M KOH	$C_g = \frac{I\Delta t}{m\Delta V}$	859 at 0.5 A g^{-1}	691 at 100 mV s^{-1}	2016[S16]
Fe_2O_3-QDs-3D GF	734	2 M KOH	$C_g = \frac{I\Delta t}{m\Delta V}$	1014 at 1.0 A g^{-1}	732 at 30 A g^{-1}	**This work**
			$C_g = \frac{2I_m\int V dt}{V^2\Big\vert_{V_i}^{V_f}}$	945 at 1.0 A g^{-1}	677 at 30 A g^{-1}	

[a]*SSA*: specific surface area, [b]C_g: gravimetric capacitance. [c]Note: the non-linear galvanostatic discharging plots present typical battery-like features. Therefore, $C = \Delta Q/\Delta V = I\Delta t/\Delta V$ is not applicable for calculating the capacitance[S4, S5]. Using such an equation ($C = I\Delta t/\Delta V$) will usually overestimate the specific capacitance for discharging. In this work, the C_g is calculated according to Equation (S2). To show the contrast, the C_g is also calculated according to the Equation (S3).

It is clear that our as-prepared electrode is superior to those of its most recent counterparts with high performance.

Table S3 Comparison of the electrical conductivity of 3D GF with those of typical self-assembled 3D graphene samples.

Samples	Test method	Conductivity (S m^{-1})	Ref.
Graphene aerogel	Four probe	~100	S17
Graphene hydrogel	Four probe	110	S18
3D graphene monoliths		87	S19
Graphene xerogel		500	S20
Honeycomb-like 3D graphene		649	S21
Honeycomb-like 3D graphene		~0.12	S22
Graphene hydrogel films		192	S23
3D graphene-based bulk materials		~100	S24
3D porous graphene films		1024	S25
Graphene fibers		800-1000	S26
3D graphene aerogels	Four probe	1	S27
3D hierarchical porous graphene/carbon composite		152	S28
3D GF	Four probe	1400	**This work**

It is clear that our as-prepared 3D GF is superior to most typical self-assembled 3D graphene materials in the literature.

Table S4. Impedance parameters of the electrodes with the three Fe_2O_3-QDs-3D GF composites, and the 3D GF, and pure Fe_2O_3 electrodes.

Samples	R_s (Ω)	R_{ct} (Ω)
Fe_2O_3-QDs-3D GF	1.1	0.36
Fe_2O_3-QDs-3D GF-1	1.0	0.32
Fe_2O_3-QDs-3D GF-2	1.3	1.3
3D GF	1.0	0.30
Pure Fe_2O_3	2.5	8.0

Table S5. Impedance parameters of the Fe_2O_3-QDs-3D GF//3D HPG ASC before and after the cycling stability testing for 12000 cycles at 20 A g^{-1}.

Samples	R_s (Ω)	R_{ct} (Ω)
Before	0.60	1.1
After 12000 cycles at 20 A g^{-1}	0.68	1.1

References

S1 Y. Y. Li, Z. S. Li, P. K. Shen, *Adv. Mater.*, 2013, **25**, 2474-2480.

S2 H. Zhang, Q. Gao, K. Yang, Y. Tan, W. Tian, L. Zhu, Z. Li, C. Yang, *J. Mater.*

Chem. A, 2015, **3**, 22005-22011.

S3 J. Chen, J. Xu, S. Zhou, N. Zhao, C.-P. Wong, *Nano Energy*, 2015, **15**, 719-728.

S4 L. Q. Mai, A. Minhas-Khan, X. Tian, K. M. Hercule, Y.-L. Zhao, X. Lin, X. Xu, *Nat. Commun.*, 2013, **4**, 2923.

S5 B. Akinwolemiwa, C. Peng, G. Z. Chen, *J. Electrochem. Soc*., 2015, **162**, A5054-A5059.

S6 X. Xia, Q. Hao, W. Lei, W. Wang, D. Sun, X. Wang, *J. Mater. Chem*., 2012, **22**, 16844-16850.

S7 W. Yang, Z. Gao, J. Wang, B. Wang, L. Liu, *Solid State Sci*., 2013, **20**, 46-53.

S8 Z. Wang, C. Ma, H. Wang, Z. Liu, Z. Hao, *J. Alloys. Compd*., 2013, **552**, 486-491.

S9 Z. Ma, X. Huang, S. Dou, J. Wu, S. Wang, *J. Phys. Chem. C*, 2014, **118**, 17231-17239.

S10 S. Yang, X. Song, P. Zhang, J. Sun, L. Gao, *Small*, 2014, **10**, 2270-2279.

S11 H. Wang, Z. Xu, H. Yi, H. Wei, Z. Guo, X. Wang, *Nano Energy*, 2014, **7**, 86-96.

S12 H. Liu, J. Zhang, D. Xu, L. Huang, S. Tan, W. Mai, *J. Solid State Electrochem*., 2015, **19**, 135-144.

S13 S. Yang, X. Song, P. Zhang, L. Gao, *ACS Appl. Mater. Interfaces*, 2015, **7**, 75-79.

S14 H. Xia, C. Hong, B. Li, B. Zhao, Z. Lin, M. Zheng, S. V. Savilov, S. M. Aldoshin, *Adv. Funct. Mater*., 2015, **25**, 627-635.

S15 C. Guan, J. Liu, Y. Wang, L. Mao, Z. Fan, Z. Shen, H. Zhang, J. Wang, *ACS Nano*, 2015, **9**, 5198-5207.

S16 M. M. Islam, D. Cardillo, T. Akhter, S. H. Aboutalebi, H. K. Liu, K. Konstantinov, S. X. Dou, *Part. Part. Syst. Character*., 2016, **33**, 27-37.

S17 M. A. Worsley, P. J. Pauzauskie, T. Y. Olson, J. Biener, J. H. Satcher Jr, T. F. Baumann, *J. Am. Chem. Soc*., 2010, **132**, 14067-14069.

S18 W. Chen, L. Yan, *Nanoscale*, 2011, **3**, 3132-3137.

S19 M. A. Worsley, T. Y. Olson, J. R. Lee, T. M. Willey, M. H. Nielsen, S. K. Roberts, P. J. Pauzauskie, J. Biener, J. H. Satcher Jr, T. F. Baumann, *J. Phys. Chem. Lett*., 2011, **2**, 921-925.

S20 H. D. Pham, V. H. Pham, T. V. Cuong, T.-D. Nguyen-Phan, J. S. Chung, E. W. Shin, S. Kim, *Chem. Commun.*, 2011, **47**, 9672-9674.

S21 S. H. Lee, H. W. Kim, J. O. Hwang, W. J. Lee, J. Kwon, C. W. Bielawski, R. S. Ruoff, S. O. Kim, *Angew. Chem. Int. Edit.*, 2010, **122**, 10282-10286.

S22 L. Qiu, J. Z. Liu, S. L. Chang, Y. Wu, D. Li, *Nat. Commun.*, 2012, **3**, 1241.

S23 Y. Xu, Z. Lin, X. Huang, Y. Liu, Y. Huang, X. Duan, *ACS Nano*, 2013, **7**, 4042-4049.

S24 L. Zhang, F. Zhang, X. Yang, G. Long, Y. Wu, T. Zhang, K. Leng, Y. Huang, Y. Ma, A. Yu, *Sci. Rep.*, 2013, **3**, 1408.

S25 B. G. Choi, M. Yang, W. H. Hong, J. W. Choi, Y. S. Huh, *ACS Nano*, 2012, **6**, 4020-4028.

S26 Y. Zhao, C. Jiang, C. Hu, Z. Dong, J. Xue, Y. Meng, N. Zheng, P. Chen, L. Qu, *ACS Nano*, 2013, **7**, 2406-2412.

S27 G. Tang, Z.-G. Jiang, X. Li, H.-B. Zhang, A. Dasari, Z.-Z. Yu, *Carbon*, 2014, **77**,

592-599.

S28 X. J. Li, W. Xing, J. Zhou, G. Q. Wang, S. P. Zhuo, Z. F. Yan, Q. Z. Xue, S. Z. Qiao, *Chem. Eur. J.*, 2014, **20**, 13314-13320.